Indium (III) chloride inhibits testicular Leydig cell proliferation by disrupting centrosome copy numbers

CHIA-YIH WANG[1,2*], PING-JUI SU[3*], KUAN-CHIH WANG[4*], RUEI-CI LIN[1,2], MIN-YUN KE[1,5] and YEN-NI TENG[5]

[1]Department of Cell Biology and Anatomy, College of Medicine, National Cheng Kung University, Tainan 701, Taiwan, R.O.C.; [2]Institute of Basic Medical Sciences, College of Medicine, National Cheng Kung University, Tainan 701, Taiwan, R.O.C.; [3]Division of General Surgery, Department of Surgery, National Cheng Kung University Hospital, Tainan 701, Taiwan, R.O.C.; [4]Division of Plastic and Reconstructive Surgery, Department of Surgery, An-Nan Hospital, China Medical University, Tainan 709, Taiwan, R.O.C.; [5]Department of Biological Sciences and Technology, National University of Tainan, Tainan 700, Taiwan, R.O.C.

Received August 4, 2025; Accepted February 17, 2026

DOI: 10.3892/mmr.2026.13891

Abstract. Indium chloride ($InCl_3$), widely used in the electronics and semiconductor industries, has recently been shown to impair testicular development and cause sperm malformations, contributing to male infertility. While testicular Leydig cells are key in testis development and testosterone biosynthesis, the effects of $InCl_3$ on Leydig cell proliferation remain unclear. The present study demonstrated that $InCl_3$ suppresses the proliferation of testicular Leydig cells by disrupting centrosome number regulation. As the centrosome is pivotal in organizing microtubules and forming the mitotic spindle during cell division, $InCl_3$-induced centrosome amplification leads to abnormal spindle formation and genomic instability. Mechanistically, $InCl_3$ increases reactive oxygen species production, resulting in DNA damage and subsequent activation of DNA-dependent protein kinase (DNA-PK), which localizes to the centrosome. Inhibition or knockdown of DNA-PK attenuated $InCl_3$-induced centrosome amplification. Additionally, induction of autophagy was observed upon $InCl_3$ exposure and pharmacological inhibition of autophagy using chloroquine suppressed centrosome amplification. Overall, the present findings reveal that $InCl_3$ inhibits Leydig cell proliferation by promoting centrosome amplification and highlights the involvement of DNA-PK activation and autophagy in this process.

Correspondence to: Dr Yen-Ni Teng, Department of Biological Sciences and Technology, National University of Tainan, Section 2, 33 Shu-Lin Street, Tainan 700, Taiwan, R.O.C.
E-mail: tengyenni1968@gmail.com

*Contributed equally

Abbreviations: InCl3, indium chloride; ATM, ataxia telangiectasia mutated; ATR, ATM and Rad3-related kinase; DNA-PK, DNA-dependent protein kinase; DNA-PKcs: DNA-PK catalytic subunit; NAC, N-acetyl-L-cysteine; DCFH-DA, 2',7'-dichlorofluorescin diacetate; ROS, reactive oxygen species; DDR, DNA damage response; DPI, diphenyleneiodonium; siRNA, small-interfering RNA; γ-H2AX, γ-H2A histone family member X; ATG7, autophagy related 7

Key words: indium chloride, testicular Leydig cell, proliferation, centrosome, DNA-dependent protein kinase

Introduction

Indium, a group IIIA element of the periodic table, is a rare earth metal characterized by its low resistance, high thermal conductivity, corrosion resistance, light permeability and electrical conductivity (1). Indium is employed in electronics, optoelectronics, defense aerospace, nuclear power, semiconductor manufacturing and other industries. Occupational exposure to indium-containing particles has increased in previous years due to the rising demand for consumer electronics (2,3). Consequently, an increasing number of diseases associated with occupational indium exposure have been reported (4-6). Indium compounds can be ingested or inhaled into the human body and are excreted through urine. The biological half-life of indium is ~2 weeks. Acute exposure to indium can damage the eyes, skin, mucosal epithelium and the respiratory system (7). Chronic exposure, particularly through inhalation of a number of indium-containing compounds, such as indium-tin oxide or indium oxide, leads to fatal interstitial pneumonia. In animal experiments, long-term exposure to indium has been shown to affect the functions of the kidneys, liver, heart, lungs and blood as well as cause embryotoxicity and fetal malformations (8,9). Previous studies have also found that continuous exposure to indium chloride ($InCl_3$) leads to abnormal male reproductive function. For example, $InCl_3$ impacts male fertility by causing DNA damage in sperm. In addition, $InCl_3$ also affects testicular development; however, the underlying molecular mechanisms remain unclear (10,11).

Anatomically, the testes are divided into numerous testicular lobules by the invaginating tunica albuginea, each containing coiled seminiferous tubules for sperm production (12). The interstitial space between seminiferous tubules consists of loose connective tissue containing testicular Leydig cells, which are responsible for testosterone biosynthesis. In male mammals, ~95% of testosterone in the body

is synthesized and secreted by Leydig cells (13). Therefore, Leydig cells are important for the development of secondary sexual characteristics and germ cell differentiation (14). These cells are key in the proper development of the fetal testis. Damage to Leydig cells impairs testicular development and in severe cases, leads to male infertility.

The mechanisms by which indium induces tissue damage remain largely underexplored. However, numerous studies have suggested that excessive production of reactive oxygen species (ROS) serves a central role in this process (15-17). Excessive ROS induce oxidative stress, resulting in severe DNA damage. When DNA damage is not adequately repaired, genomic instability ensues (18). In response to DNA damage, cells activate DNA damage response (DDR) pathways to repair the genome. Furthermore, when the extent of damage exceeds the repair capacity of the cells, cell death is triggered to eliminate the affected cells.

DDR generally involves the recognition of DNA lesions and the initiation of signaling cascades that promote repair and arrest cell cycle progression. DNA damage signaling is primarily mediated through protein phosphorylation. A total of three key members of the PI3K-related kinase family, ataxia-telangiectasia mutated (ATM), ataxia telangiectasia and Rad3-related (ATR) and DNA-dependent protein kinase (DNA-PK), serve as principal regulators of the DDR (19). ATM acts as a central kinase orchestrating the cellular response to double-strand breaks by regulating DNA repair, checkpoint activation, apoptosis and senescence (20). Upon single-strand breaks, ATR is recruited to extended tracts of single-stranded DNA coated with replication protein A to promote DNA repair (21). DNA-PK is composed of a catalytic subunit (DNA-PKcs) and a regulatory heterodimer (Ku70/Ku80) (22). When sensing DNA double-strand breaks, Ku70/Ku80 binds to the DNA ends and recruits DNA-PKcs, forming the active DNA-PK complex. The primary role of DDR is to repair damaged DNA and halt cell cycle progression, as if the damage proves irreparable, the DDR machinery can initiate apoptotic signaling to eliminate the compromised cells.

ROS also activates autophagy, which promotes either cell survival by facilitating damaged organelle removal and metabolic adaptation, or instead contributes to cell death when excessively activated or when degradation fails (23). Autophagy is a catabolic process and a key pathway involved in removing damaged organelles, such as mitochondria (24). Upon autophagy initiation, the mTOR pathway is inhibited, which leads to the activation of unc-51-like autophagy activating kinase 1/2 complexes, initiating the autophagy cascade (25). Subsequently, the class III PI3K complex is activated to promote formation of the phagophore, and LC3 is cleaved by autophagy-related (ATG)-4 to expose the C-terminal glycine residue at position 116 (LC3-I). LC3-I is conjugated to phosphatidylethanolamine forming LC3-II, which is inserted into both the inner and outer autophagosomal membranes and thereby facilitates phagophore elongation, cargo sequestration and closure of the autophagosome (26). Once formed, the autophagosome fuses with the lysosome, leading to the degradation of sequestered cytoplasmic components.

The centrosome is the microtubule organization center of the cell. It is composed of a pair of centrioles and pericentriolar material which encompasses the surrounding protein matrix. This pair of centrioles includes a mother centriole and a daughter centriole (27). During interphase of the cell cycle, the centrosome orchestrates the microtubule networks to maintain the shape of the cell and guide the direction of the cell migration. When the cell enters the mitotic phase, the duplicated centrosomes move to the opposite sites of the nucleus and form mitotic spindle poles to promote chromosomal arrangement on the equatorial plate (28). During cell cycle progression, each cell contains one centrosome (before duplication) or two centrosomes (after duplication). However, when cells suffer from environmental or intercellular stresses, the centrosome undergoes amplification (cells with >2 centrosomes), thus leading to aberrant mitotic spindle poles and genomic instability. Therefore, precise control of the number of centrosomes stabilizes the inheritance of the cell genome for undisturbed cell proliferation (29).

The present study aimed to uncover the molecular mechanism by which $InCl_3$ inhibits testicular cell proliferation. The present study aimed to elucidate the molecular mechanisms by which InCl3 inhibits testicular Leydig cell proliferation, with a particular focus on whether excessive ROS production, DNA-PK activation, centrosome amplification and autophagy are involved in this process.

Materials and methods

Cell culture and drug treatment. Mouse progenitor Leydig TM3 cells and tumor Leydig MA-10 cells were maintained in DMEM-F12 medium (Invitrogen; Thermo Fisher Scientific, Inc.), supplemented with 10% FBS (Thermo Fisher Scientific, Inc.), 1% sodium pyruvate (Thermo Fisher Scientific, Inc.) and 100 IU/ml penicillin-streptomycin (Thermo Fisher Scientific, Inc.) at 37˚C under a humidified atmosphere with 5% CO_2. Leydig cells were exposed to the following drugs for the durations indicated in the results section: $InCl_3$ (10, 20, 50, 100 or 200 μM; cat. no. 203440; Sigma-Aldrich; Merck KGaA), the ROS scavenger N-acetyl-L-cysteine (NAC; cat. no. A9165; Sigma-Aldrich; Merck KGaA), the DNA-PK inhibitor vanillin (1 μM; cat.no. V110-4; Sigma-Aldrich; Merck KGaA), 2',7'-dichlorofluorescin diacetate (DCFH-DA; cat. no. D6883; Sigma-Aldrich; Merck KGaA), diphenyleneiodonium (DPI; 10 μM; cat. no. D2926; Sigma-Aldrich; Merck KGaA), Mito-TEMPO (10 μM; cat. no. SML0737; Sigma-Aldrich; Merck KGaA) and the autophagy inhibitor chloroquine (100 μM; cat. no. NBP2-29386; Novus Biologicals; Bio-Techne).

Small-interfering RNA (siRNA) transfection. siRNAs against DNA-PKcs (siDNA-PKcs) and ATG7 (siATG7) were purchased from Sigma-Aldrich; Merck KGaA. The sequences of siRNAs were as follows: siDNA-PKcs, sense, 5'-CCUUCA GUACGAUUAGCGCCC-3'; antisense, 5'-GGGCGCUAA UCGUACUGAAGG-3'; siATG7, sense, 5'-CCGUUCAUU GAUCAAGAACCC-3'; antisense, 5'-GGUUCUUGAUCA AUAUGAACG-3'; and scrambled siRNA, sense, 5'-UCUGAU CGCACGUAUGAUCUU-3'; antisense, 5'-GAUCAUACG UGCGAUCAGAUU-3'.

For siRNA transfection, Lipofectamine 2000™ (Invitrogen; Thermo Fisher Scientific, Inc.) was mixed with

Opti-MEM (Thermo Fisher Scientific, Inc.), followed by the addition of 100 nM siRNA. The mixture was then incubated at room temperature for 25 min before being applied to the cells. Cells were harvested at room temperature 72 h post-transfection for further experiments.

Western blotting. Cells were harvested through trypsinization and lysed on ice for 10 min using the CelLytic™ MT cell lysis reagent (Sigma-Aldrich; Merck KGaA) supplemented with a commercial protease inhibitor cocktail (P8340; Sigma-Aldrich; Merck KGaA). The lysates were centrifuged at 13,000 x g for 10 min at 4˚C and the supernatants were collected. Protein concentrations were determined using the Bio-Rad Protein Assay Kit (Bio-Rad Laboratories, Inc.). Equal amounts of protein (50 μg/lane) were mixed with 2X SDS sample buffer, boiled at 100˚C for 10 min and separated by 10% SDS-PAGE at 150 V for 90 min. Proteins were transferred onto PVDF membranes at 20 V and 4˚C overnight. Membranes were blocked with 3% BSA in TBST (containing 0.1% Tween-20) for 1 h at room temperature and incubated with primary antibodies overnight at 4˚C. After washing with TBST for 30 min, membranes were incubated with HRP-conjugated secondary antibodies for 1 h at room temperature. Primary (1:7,000) and secondary (1:7,000) antibody details are provided in Table I. Immunoreactive bands were visualized using an ECL detection kit (Thermo Fisher Scientific, Inc.).

Immunofluorescence microscopy. Following the aforementioned experimental treatments, cells were fixed and permeabilized with ice-cold methanol for 5 min. Following permeabilization, cells were incubated in a blocking buffer containing Triton X-100, Tween-20 and normal goat serum (Thermo Fisher Scientific, Inc.) for 1 h at room temperature. Primary antibodies were then applied and incubated overnight at 4˚C. The next day, cells were washed three times with PBS for a total of 30 min and subsequently incubated for 1 h at room temperature with FITC- or Cy3-conjugated goat anti-mouse or anti-rabbit IgG secondary antibodies (cat. nos. ab175473 and ab150077; Abcam) in the presence of DAPI for nuclear staining. Primary (1:200) and secondary (1:500) antibody details are provided in Table I. Afterward, cells were washed three additional times with PBS for a total of 30 min. Coverslips were mounted onto slides using 50% glycerol in PBS and fluorescence signals were visualized using an Axio Imager D2 fluorescence microscope (Zeiss AG).

Cell proliferation assay. TM3 cells were cultured at a density of $1x10^5$ cells on culture dishes. After incubation at 37˚C for 24, 48 and 72 h, cells were trypsinized and resuspended with PBS for counting cell numbers using a hemocytometer under a light microscope (Zeiss AG). All treatments were performed in triplicate, with each experiment performed three times.

Flow cytometry. Cell cycle distribution was determined by FACS flow cytometry. Briefly, TM3 cells were harvested by trypsinization and resuspended in PBS containing 1 mM EDTA (PBS-E). The cells were centrifuged at 200 x g for 5 min at 4˚C and the pellets were washed once with PBS-E. After a second centrifugation at 200 x g for 5 min at 4˚C, the cells were resuspended in 0.5 ml PBS-E and fixed by adding 4.5 ml 70% ice-cold ethanol dropwise with gentle vortexing at 4˚C. Cells were stored at 4˚C for 18 h. Before analysis, fixed cells were washed thoroughly with PBS-E to remove ethanol and then stained with propidium iodide (SouthernBiotech) for 1 h at room temperature in the dark. DNA content was measured using a FACScan flow cytometer (BD Biosciences) and data were analyzed using Kaluza software version 2.1.3 (Beckman Coulter, Inc.).

5-Ethynyl-2'-deoxyuridine (EdU) incorporation assay. TM3 cells were seeded on 25x25 mm coverslips in 6-well tissue culture plates and treated with $InCl_3$. Cell proliferation was assessed using the Click-iT™ EdU Imaging Kit (Thermo Fisher Scientific, Inc.). Briefly, 1 μl 10 μM EdU working solution (Component A) was added to the culture medium and cells were incubated for 1 h at 37˚C. After incubation, cells were fixed and permeabilized with ice-cold methanol for 5 min. The Click-iT™ EdU reaction cocktail was prepared according to the manufacturer's instructions and added to the cells for 1 h at room temperature in the dark. Following labeling, cells were washed three times with PBS for a total of 30 min. EdU signals were visualized using an Axio Imager D2 fluorescence microscope (Zeiss AG).

Enzyme-linked immunosorbent assay (ELISA). Mouse serum testosterone levels were quantified using a commercially available Mouse T Testosterone ELISA kit (cat. no. EM1850-HS; Wuhan Fine Biotech Co., Ltd.), according to the manufacturer's instructions. Briefly, the medium was collected at room temperature, then centrifuged at 1,000 x g for 20 min at 4˚C to obtain supernatant, which was either assayed immediately or stored at -80˚C until analysis. Standards were prepared by serial dilution to yield a calibration range of 31.25-2,000 pg/ml. For each assay, 50 μl samples were added in duplicate to the T-pre-coated 96-well plate, followed by 50 μl biotin-labeled detection antibody and incubated for 45 min at 37˚C. After three washes with wash buffer, 100 μl HRP-streptavidin conjugate was added to each well and incubated for 30 min at 37˚C. Plates were then washed five times, and 90 μl TMB substrate was added and incubated in the dark at 37˚C for 10-20 min, followed by the addition of 50 μl stop solution to terminate the reaction. Absorbance was measured at 450 nm using a microplate reader.

Reverse transcription-quantitative PCR. Total RNA was isolated from TM3 cells treated with or without $InCl_3$ using TRI Reagent® (Sigma-Aldrich; Merck KGaA) followed by purification with the Direct-zol™ RNA Miniprep Kit (Zymo Research Corporation.). After extraction, RNAs (1 μg) were reverse-transcribed into cDNA using the SensiFAST™ cDNA Synthesis Kit (Bioline; Meridian Bioscience) according to the manufacturer's instructions.

Quantitative PCR was performed using FastStart™ SYBR Green Master Mix (MilliporeSigma) with gene-specific primers at a final concentration of 0.25 μM. The primer sequences used for mRNA expression analysis were as follows: Cytochrome P450 family 11 subfamily A member 1 (CYP11A1) forward, 5'-GATCCCGAGGCCCAGCGGTT-3'; reverse, 5'-AGGGTC ATGGAGGTCGTGTCCA-3'; steroidogenic acute regulatory protein (StAR) forward, 5'-CAGCACTCAGCATGTTCC TCGCT-3'; reverse, 5'-TCCCCGTTCTCCTGCTGGCTTT-3'; 3-β-hydroxy-δ(5)-steroid dehydrogenase (HSD3B) forward,

Table I. Antibodies used for WB and IF.

Antibody	Company	Cat. no.	Application
Actin	MilliporeSigma	MAB1501	WB
GAPDH	GeneTex, Inc.	GTX627408	WB
HSC70	GeneTex, Inc.	GTX637440	WB
γ-tubulin	GeneTex, Inc.	GTX629704	IF
α-tubulin	GeneTex, Inc.	GTX112141	WB
Cyclin A	Abcam	ab38	WB
Cyclin D	Thermo Fisher Scientific, Inc.	2G3G5	WB
Cyclin E	Cell Signaling Technology, Inc.	4132	WB
LC3A/B	Cell Signaling Technology, Inc.	12741	WB
p-ATM (S1981)	Abcam	Ab81292	WB
ATM	GeneTex, Inc.	GTX70103	WB
p-ATR (S428)	Cell Signaling Technology, Inc.	2853	WB
ATR	GeneTex, Inc.	GTX128146	WB
p-DNA-PKcs (T2609)	GeneTex, Inc.	GTX24194	WB and IF
DNA-PKcs	Santa Cruz Biotechnology, Inc.	sc-0951	WB
γ-H2AX	Abcam	Ab11175	IF

WB, western blotting; IF, immunofluorescence staining; p-, phosphorylated; ATM, ataxia-telangiectasia mutated; ATR, ataxia telangiectasia and Rad3-related; DNA-PKcs, DNA-dependent protein kinase catalytic subunit; γ-H2AX, γ-H2A histone family member X.

5'-TCATTCCCAGGCAGACCATCC-3'; reverse, 5'-CCCTGCAACATCAACTGAGCTG-3'; and GAPDH forward, 5'-TTTGGCATTGTGGAAGGGCTC-3'; reverse, 5'-CATCACGCCACAGCTTTCCAG-3'.

All reactions were performed in triplicate in a final reaction volume of 20 μl. The cycling conditions were as follows: i) Initial denaturation at 95˚C for 2 min; ii) 40 cycles of 95˚C for 5 sec; and iii) 60˚C for 20 sec. Melt-curve analysis was conducted to verify amplification specificity. Relative mRNA expression levels were calculated using the $2^{-\Delta\Delta Cq}$ method (30) after normalization to GAPDH as the internal reference.

Statistical analysis. Data are presented as the mean ± SEM. Comparisons between two groups were performed using unpaired Student's t-tests, while comparisons among multiple groups were analyzed using one-way ANOVA tests followed by Tukey's post hoc test for multiple comparisons. $P<0.05$ was considered to indicate a statistically significant difference.

Results

$InCl_3$ inhibits testicular Leydig cell proliferation. To investigate the effects of $InCl_3$ on testicular Leydig cell proliferation, mouse progenitor Leydig TM3 cells were treated with a number of concentrations of $InCl_3$ (10, 20, 50, 100 or 200 μM) for 24, 48 or 72 h, followed by cell counting. Results demonstrated that the IC_{50} value of $InCl_3$ on TM3 cell proliferation was ~100 μM after 48 h treatment (Fig. 1A). Therefore, this condition was used for the subsequent experiments. The effect of $InCl_3$ on an additional Leydig cell line, MA-10, was examined. Treatment with 100 μM $InCl_3$ inhibited MA-10 cell growth in a time-dependent manner (Fig. 1B). These findings indicated that $InCl_3$ suppressed Leydig cell proliferation.

Subsequently, cell cycle profiles were analyzed using flow cytometry. The proportion of cells in the G_0/G_1 and S-phases was reduced, while those in the G_2/M and polyploidy phases were increased (Fig. 1C), suggesting that cell cycle progression was impaired. Given that cell cycle progression is regulated by cyclin/CDK2 complexes (10), the expression of cyclins and the activation status of CDK2 were examined. Upon $InCl_3$ treatment, the levels of cyclins D, A and E, as well as the active form of CDK2 (phosphorylated at Thr161), were reduced (Fig. 1D), supporting the conclusion that cell cycle progression was inhibited. To further demonstrate this defect, S-phase entry was assessed using an EdU incorporation assay. Compared with the control cells, the proportion of EdU-positive cells was significantly decreased in $InCl_3$-treated TM3 cells (Fig. 1E and F). Collectively, these results indicated that $InCl_3$ inhibits the proliferation of Leydig TM3 cells by impairing cell cycle progression.

Flow cytometry analysis revealed an increased proportion of polyploid cells, therefore the nuclear morphology was examined. Following $InCl_3$ treatment, TM3 cells exhibited irregularly shaped nuclei (Fig. 2A) and a significant increase in nuclear size was also observed in $InCl_3$-treated cells (Fig. 2B). Additionally, the higher percentage of cells with micronuclei (small, extranuclear DNA-containing bodies near the nucleus, as indicated by arrowheads in Fig. 2C) observed, suggested that genomic instability had been induced. As genomic instability is associated with defective mitotic entry, the ability of cells to enter mitosis was assessed by measuring the mitotic index, defined as the percentage of cells in mitosis. Cells undergoing mitosis were identified by DAPI staining, which reveals condensed chromosomes with increased fluorescence intensity. Findings showed that the mitotic index was not significantly affected by $InCl_3$ treatment (Fig. 2D), suggesting

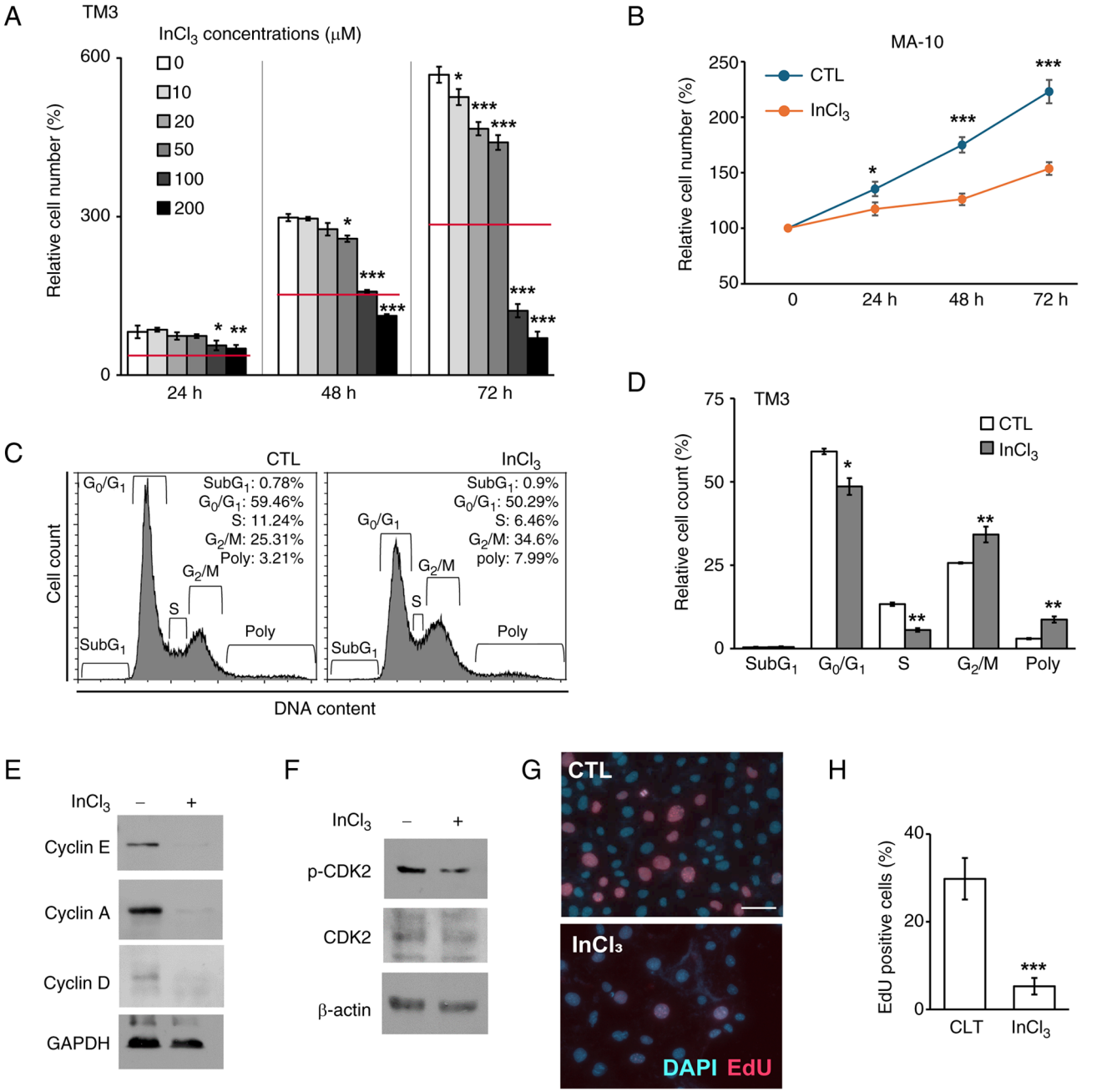

Figure 1. $InCl_3$ inhibits TM3 cell proliferation. (A) $InCl_3$ inhibited TM3 cell growth in a time- and dose-dependent manner. Quantitative results of relative cell numbers upon $InCl_3$ treatment at different dosages and periods. (B) $InCl_3$ inhibited MA-10 cell proliferation in a time-dependent manner. Quantitative results of relative cell numbers upon $InCl_3$ (100 μM) treatment at different periods. (C) Cell cycle profiles shown using flow cytometry analysis. (D) Quantitative results of flow cytometry analysis. Cell cycle-related cyclins were downregulated upon $InCl_3$ treatment. Extracts of TM3 cells treated with or without $InCl_3$ were analyzed using western blotting with antibodies against (E) cyclin E, cyclin A, cyclin D, GAPDH and (F) p-CDK2, CDK2 and α-actin. $InCl_3$ inhibited S-phase entry. (G) Cell ability to enter the S-phase was analyzed using an EdU incorporation assay. (H) Quantitative results of the EdU assay. Results are presented as mean ± SD from ≥3 independent experiments. *P<0.05, **P<0.01 and ***P<0.001. $InCl_3$, indium chloride; EdU, 5-ethynyl-2'-deoxyuridine; CTL; control; p-, phosphorylated.

that the ability of cells to enter mitosis was not impaired. Collectively, these findings indicated that $InCl_3$ treatment induces genomic instability in TM3 cells.

Testicular Leydig cells synthesize testosterone through the steroidogenic pathway (31). To determine whether $InCl_3$ influences testosterone production, the levels were measured following $InCl_3$ treatment. ELISA analysis revealed a significant reduction in testosterone levels upon $InCl_3$ treatment (Fig. 2E). Furthermore, the expression levels of steroidogenic genes StAR and HSD3B, but not CYP11A11, were significantly decreased in $InCl_3$-treated cells (Fig. 2F-I). These results indicated that $InCl_3$ not only suppressed Leydig cell proliferation but also downregulated the expression of key steroidogenic genes involved in testosterone biosynthesis.

$InCl_3$ induces centrosome amplification. It has been established that aberrant mitosis facilitates genomic instability (22). Therefore, the mitotic apparatus in $InCl_3$-treated TM3 cells

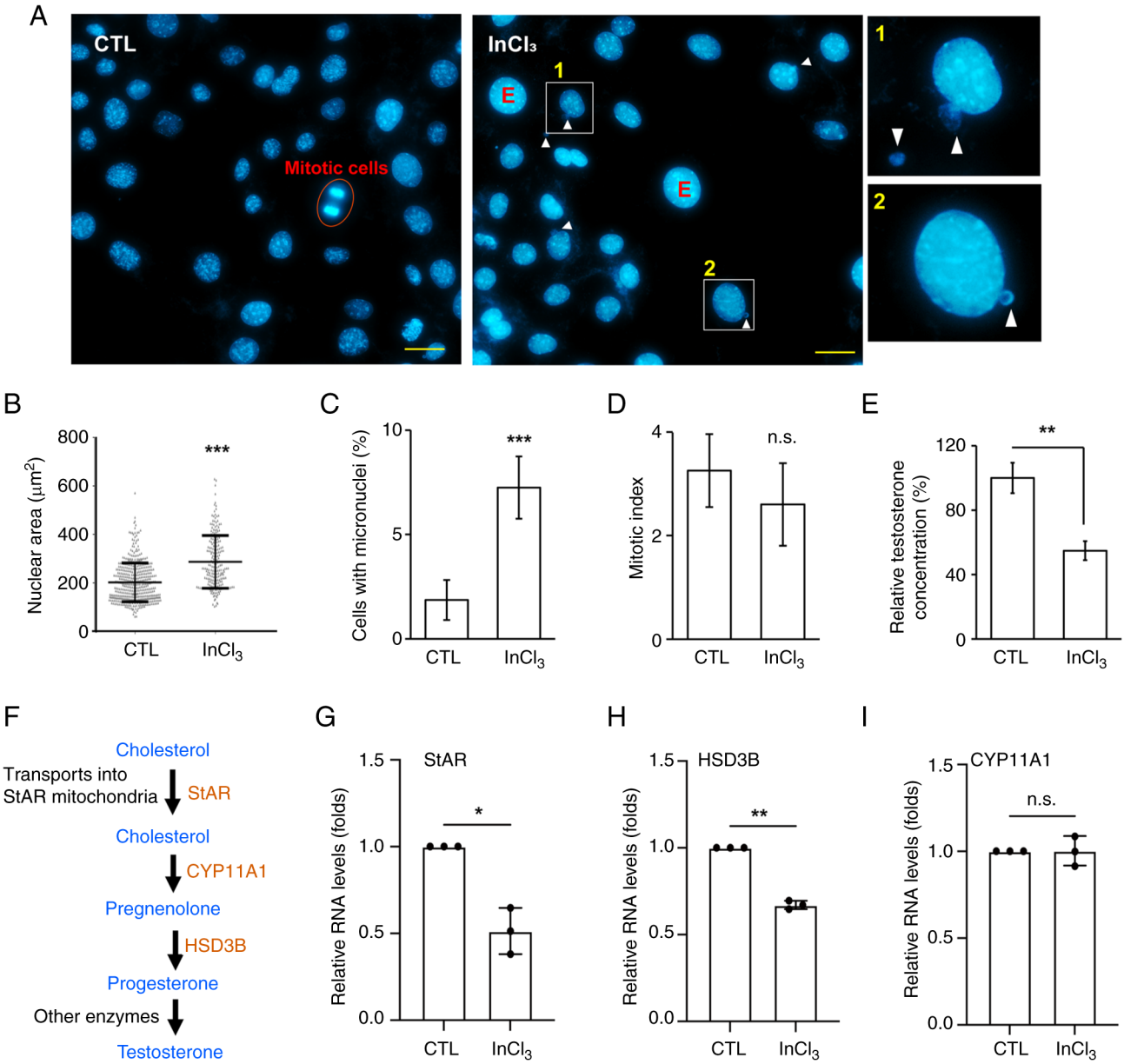

Figure 2. Genomic instability is observed in $InCl_3$-treated TM3 cells. $InCl_3$ induces enlarged nuclei and micronuclei (as indicated by white arrowheads) in TM3 cells. (A) Nuclear shapes of CTL and $InCl_3$-treated TM3 cells were analyzed using DAPI staining. The right panel represents enlarged views of selected regions. Micronuclei, small DAPI staining near the nucleus, are indicated by the arrowheads. Mitotic cells were identified and are marked with red circles. Scale bar, 10 μm. (B) Quantitative results of the nuclear area shown through DAPI staining. (C) Quantification of the proportions of cells with micronuclei [as indicated by selected regions 1 and 2 of (A), right panel]. (D) $InCl_3$ treatment did not affect the mitotic index. The proportions of mitotic cells (mitotic index) were quantified. (E) $InCl_3$ treatment reduced the levels of testosterone in the culture medium of TM3 cells. Quantitative results of relative testosterone levels measured through ELISA in the absence or presence of $InCl_3$. $InCl_3$ treatment reduced steroidogenic gene expression. (F) Schematic diagram of testosterone production. Quantitative results of relative mRNA levels of (G) StAR, (H) HSD3B and (I) CYP11A1. Results are presented as mean ± SD from ≥3 independent experiments. *P<0.05, **P<0.01 and ***P<0.001. n.s., not significant; $InCl_3$, indium chloride; StAR, steroidogenic acute regulatory protein; HSD3B, 3-β-hydroxy-δ(5)-steroid dehydrogenase; CYP11A1, cytochrome P450 family 11 subfamily A member 1; E, enlarged nuclei; CTL, control.

was investigated. Under control conditions, cells exhibited two spindle poles that aligned chromosomes at the metaphase plate (Fig. 3A, upper panel; Fig. S1A, left panel). However, upon $InCl_3$ treatment, numerous spindle poles and misaligned chromosomes were observed (Figs. 3A and B and S1A), with this phenotype also being observed in MA-10 cells (Figs. 3C and D and S1B), suggesting that $InCl_3$ treatment led to aberrant mitosis.

Given that multipolar spindles often result from centrosome amplification during interphase (32), the number of centrosomes was also assessed. Under control conditions, cells contain one centrosome before duplication and two after duplication. By contrast, $InCl_3$-treated TM3 and MA-10 cell lines exhibited a marked increase in centrosome amplification, characterized by more than two discrete γ-tubulin-positive foci per cell instead of the single pair observed in controls (Figs. 3E-H and S2A and B) at 24, 48 and 72 h, supporting the hypothesis that $InCl_3$ induces centrosome amplification. Furthermore, as centrosomes function as the microtubule-organizing centers that coordinate the

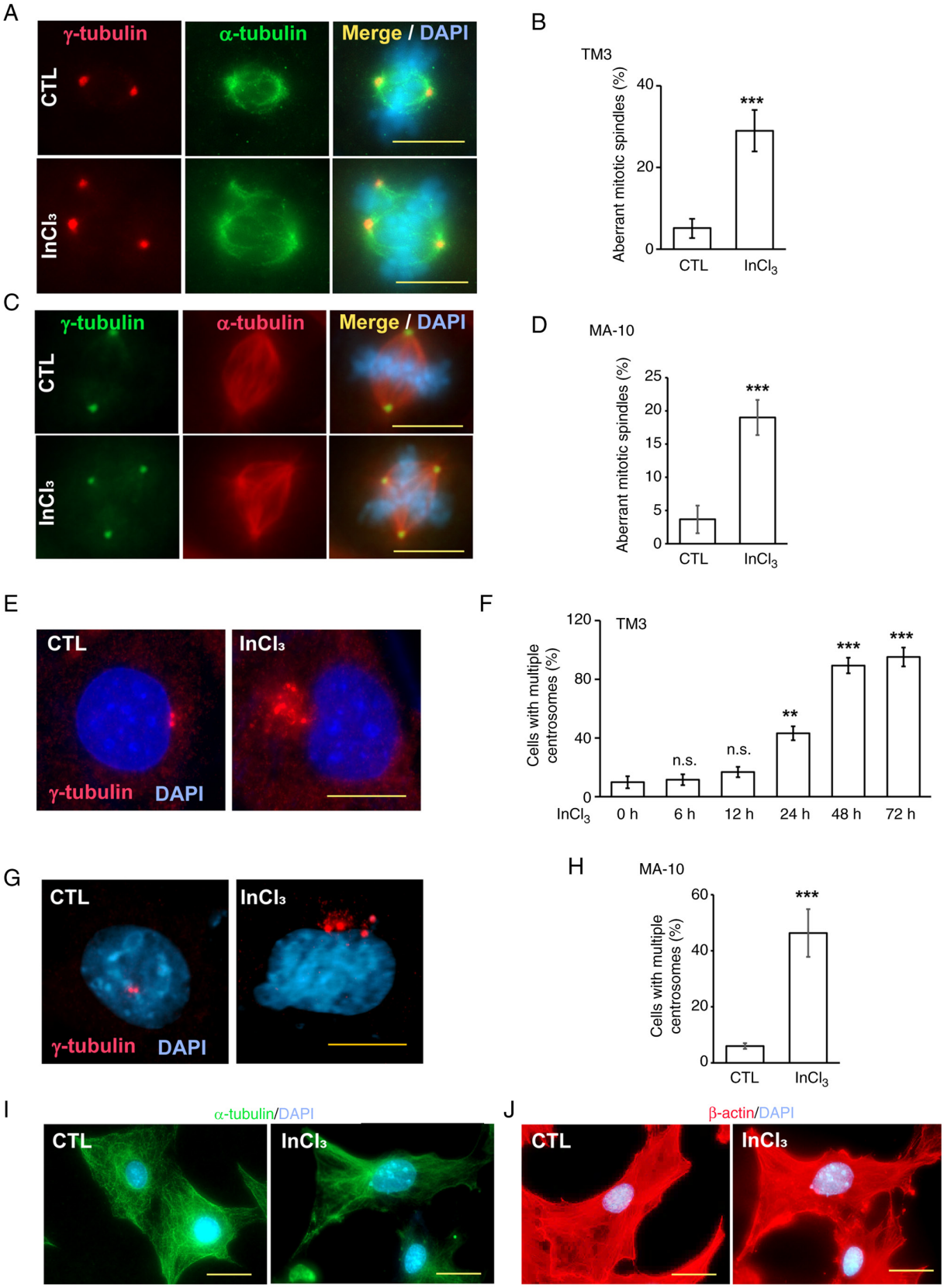

Figure 3. $InCl_3$ treatment facilitates centrosome amplification in TM3 cells. Treatment of $InCl_3$ led to aberrant mitotic spindles. Immunofluorescence staining of CTL and $InCl_3$-treated (A) TM3 cells and (C) MA-10 cells with antibodies against γ-tubulin (centrosome) and α-tubulin (mitotic spindles). DNA was stained with DAPI. Scale bars, 10 μm. Quantitative results of (B) TM3 and (D) MA-10 Leydig cells with aberrant mitosis. Treatment with $InCl_3$ induced centrosome amplification. Immunofluorescence staining of CTL or $InCl_3$-treated (E) TM3 cells and (G) MA-10 cells with antibodies against γ-tubulin. A cell with more than two centrosomes was defined as a cell with centrosome amplification. DNA was stained with DAPI. Scale bars, 10 μm. Quantitative results of cells with centrosome amplification in (F) TM3 and (H) MA-10 cell lines. (I) Treatment of $InCl_3$ resulted in disorganized microtubule arrays. Immunofluorescence staining of CTL or $InCl_3$-treated cells with antibodies against α-tubulin. DNA was stained with DAPI. Scale bar, 10 μm. (J) Treatment of $InCl_3$ did not affect actin filaments. Immunofluorescence staining of CTL or $InCl_3$-treated cells with antibodies against actin. DNA was stained with DAPI. Scale bar, 10 μm. Results are presented as mean ± SD from ≥3 independent experiments. **P<0.01 and ***P<0.001. CTL, control; $InCl_3$, indium chloride; n.s., not significant.

microtubule network, the present study further examined the microtubule organization. In control cells, a well-organized microtubule network was observed, whereas in $InCl_3$-treated cells, microtubules clustered into bundles surrounding each centrosome (Fig. 3I), suggesting disruption of the microtubule network. Additionally, analysis of the actin cytoskeleton revealed that the alignment of actin filaments was disrupted and actin puncta were present in $InCl_3$-treated cells (Fig. 3J). Together, these findings indicated that $InCl_3$ induced centrosome amplification and disrupted both microtubule networks and actin filament organization.

$InCl_3$ induces centrosome amplification via elevating ROS production. $InCl_3$ has been reported to lead to excessive ROS production in a number of cell types (7,33), however whether it induces ROS in Leydig cells remains unclear. To address this question, ROS levels were measured in $InCl_3$-treated Leydig TM3 cells using a DCFH-DA assay. $InCl_3$ treatment caused a time-dependent increase in fluorescence intensity, indicating elevated ROS production in TM3 cells (Fig. 4A).

Subsequently, the association between ROS and centrosome amplification was investigated. Notably, treatment with the ROS scavenger NAC alleviated $InCl_3$-induced centrosome amplification (Figs. 4B and S3), suggesting that ROS generation is required for this phenotype. Two selective inhibitors were used to further determine whether these ROS originate from mitochondria or cytosolic NADPH oxidase (NOX) activity, specifically Mito-TEMPO and DPI. Treatment with Mito-TEMPO, a mitochondria-targeted scavenger of mitochondrial superoxide, significantly reduced centrosome amplification (Figs. 4C and S4A). Treatment with DPI, an inhibitor that primarily suppresses NOX-dependent cytosolic ROS production, similarly attenuated $InCl_3$-induced centrosome amplification (Figs. 4D and S4B). Together, these findings suggested that $InCl_3$ induced ROS production from both mitochondrial and NOX-dependent cytosolic sources and that ROS generation from either pathway contributed to centrosome amplification.

$InCl_3$ activates DNA-PK to induce centrosome amplification. As ROS is known to cause DNA damage (34) and the DDR can induce centrosome amplification in osteosarcoma cells (22,35,36), it was hypothesized that $InCl_3$ increases ROS levels, leading to DNA damage and subsequent centrosome amplification in testicular Leydig cells. To explore this, DNA damage was assessed through the detection of γ-H2A histone family member X (γ-H2AX), a marker of DNA double-strand breaks (37). $InCl_3$ treatment significantly elevated γ-H2AX levels, as shown by both immunofluorescence staining and western blotting analysis (Fig. 4E and F), indicating that DNA damage was induced. Moreover, NAC treatment reduced γ-H2AX levels, further supporting that ROS mediates DNA damage in $InCl_3$-treated Leydig TM3 cells. Subsequently, the present study tested whether ROS contributed to centrosome amplification.

DDR signaling pathways including ATM, ATR and DNA-PK were investigated. Findings revealed that ATM and ATR were not activated by $InCl_3$ treatment (Fig. 5A and B). However, DNA-PK was activated, as evidenced by increased phosphorylation of its catalytic subunit (DNA-PKcs) following $InCl_3$ treatment (Fig. 5C). Subsequently, the time course of DNA-PK activation was investigated. The phosphorylation of DNA-PKcs increased as early as 12 h after $InCl_3$ treatment, remained elevated up to 48 h and then decreased by 72 h (Fig. 5D), suggesting transient DNA-PK activation between 12 and 48 h. Collectively, this suggests that $InCl_3$ may have activated DNA-PK in Leydig cells. The present study further investigated whether DNA-PK contributes to centrosome amplification by treating cells with the selective DNA-PK inhibitor vanillin (38). Treatment of cells with vanillin reduced $InCl_3$-induced centrosome amplification (Figs. 5E and F and S5A). To further demonstrate this, DNA-PKcs was depleted using siRNA transfection (Fig. 5G), which also alleviated $InCl_3$-induced centrosome amplification (Figs. 5H and I and S5B). Therefore, this indicated that $InCl_3$ promoted centrosome amplification through DNA-PK activation in Leydig cells.

A previous study has shown that phosphorylated DNA-PKcs localizes to the centrosome, thereby facilitating centrosome amplification (39). To determine whether this occurs upon $InCl_3$ treatment, the subcellular localization of phosphorylated DNA-PKcs was examined. Under control conditions, phosphorylated DNA-PKcs was barely detectable. However, after $InCl_3$ treatment, in addition to its nuclear localization, phosphorylated DNA-PKcs was also observed at the centrosome (Fig. 5H). Taken together, the present data suggested that $InCl_3$ induced centrosome amplification by activating DNA-PK.

$InCl_3$ activates autophagy to induce centrosome amplification. It has previously been established that DNA damage can activate autophagy (40). In addition, autophagy promotes centrosome amplification in trophoblast cells (41). Therefore, the present study examined whether $InCl_3$ activates autophagy. LC3 puncta increased markedly in TM3 cells treated with $InCl_3$ (Fig. 6A), indicating activation of autophagy. To further demonstrate this finding, LC3 lipidation was examined. $InCl_3$ treatment increased the LC3-II/LC3-I ratio (Fig. 6B, upper panel) and reduced sequestosome 1/p62 levels (Fig. 6B, lower panel), both of which are consistent with enhanced autophagic activity. When examining the lysosome, treatment with $InCl_3$ did not affect the expression of lysosomal proteins, including lysosome-associated membrane protein 1 (LAMP1) and cathepsin D (Fig. 6C). The time course of autophagy induction was next characterized. The LC3-II/LC3-I ratio increased as early as 12 h after $InCl_3$ treatment, remained elevated up to 48 h and then decreased by 72 h (Fig. 6D), suggesting transient autophagy activation between 12 and 48 h. Next, the present study investigated whether autophagy was mediated by DNA-PK activation. Treatment of cells with the DNA-PK inhibitor vanillin mitigated an increase in the LC3-II/LC3-I ratio (Fig. 6E), suggesting that DNA-PK activation promoted autophagy under $InCl_3$ treatment. Furthermore, examination of whether autophagy contributes to centrosome amplification was conducted. Pharmacological inhibition of autophagy with chloroquine attenuated $InCl_3$-induced centrosome amplification (Figs. 6F and S6A). A genetic approach was followed to further demonstrate this observation. ATG7 knockdown with siRNA (Fig. 6G) similarly reduced $InCl_3$-induced centrosome amplification (Figs. 6H and S6B). Together, these results indicated that $InCl_3$ activated autophagy, which in turn promoted centrosome amplification.

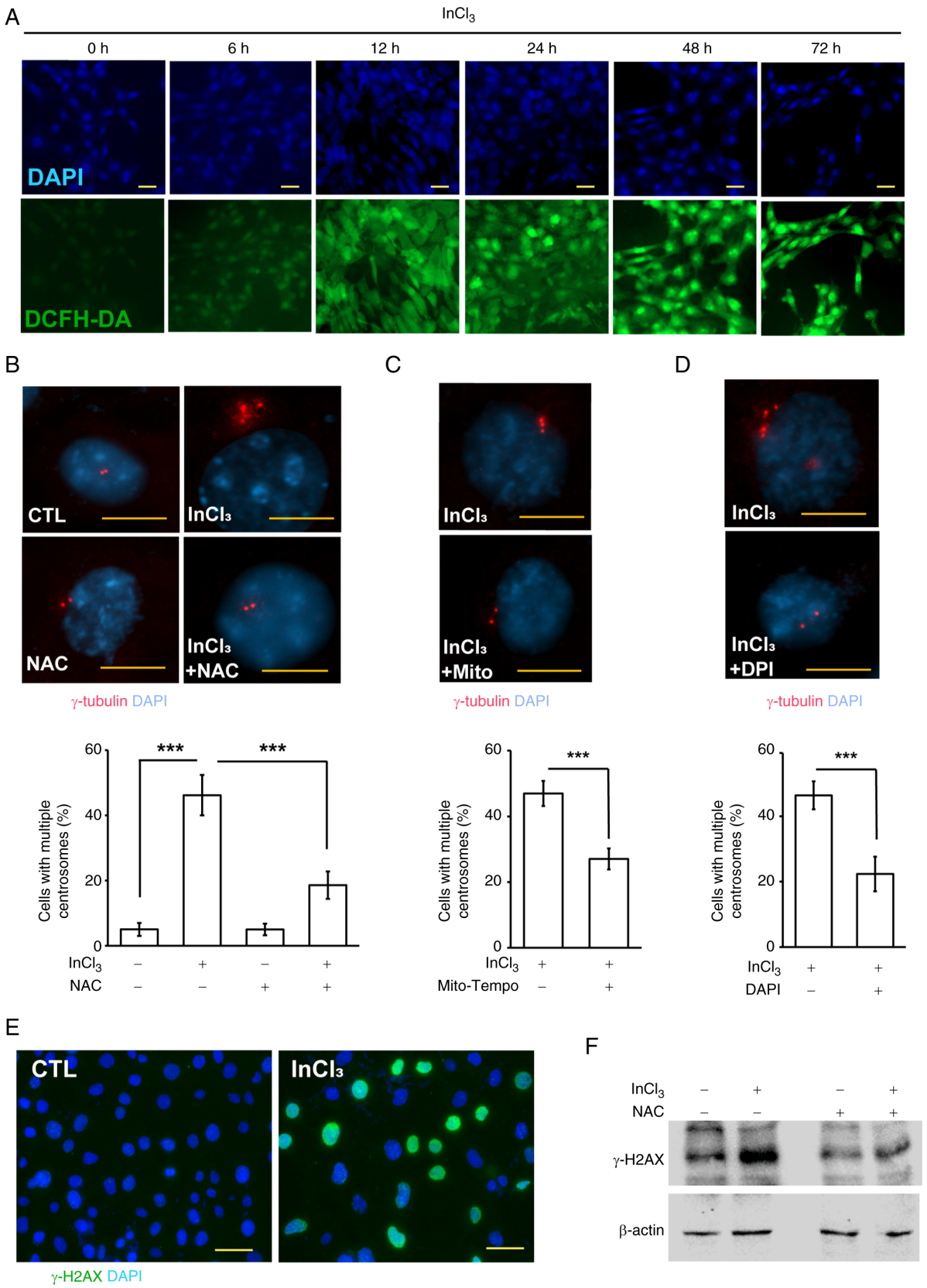

Figure 4. Treatment of $InCl_3$ induces ROS production and DNA damage. (A) $InCl_3$ induced ROS production. Immunofluorescence staining of CTL or $InCl_3$-treated cells with DCFH-DA (green, ROS-positive cells) at different time periods. DNA was stained with DAPI. Scale bars, 20 μm. Inhibition of ROS alleviated $InCl_3$-induced centrosome amplification. Representative immunofluorescence images and quantification of TM3 cells with centrosome amplification in the absence or presence of ROS inhibitors, including (B) NAC, (C) Mito-Tempo and (D) DPI. Cells were stained with an antibody against γ-tubulin. DNA was counterstained with DAPI. Scale bars, 10 μm. (E) $InCl_3$ induced DNA damage. Immunofluorescence staining of CTL or $InCl_3$-treated cells with an antibody against γ-H2AX (green). DNA was stained with DAPI. Scale bar, 20 μm. (F) Inhibition of ROS alleviated $InCl_3$-induced DNA damage. Extracts of TM3 cells in the absence or presence of ROS inhibitor (NAC) were analyzed through western blotting with antibodies against γ-H2AX and actin. Results are presented as mean ± SD from ≥3 independent experiments. ***P<0.001. ROS, reactive oxygen species; $InCl_3$, indium chloride; NAC, N-acetyl-L-cysteine; DPI, diphenyleneiodonium; γ-H2AX, γ-H2A histone family member X; CTL, control.

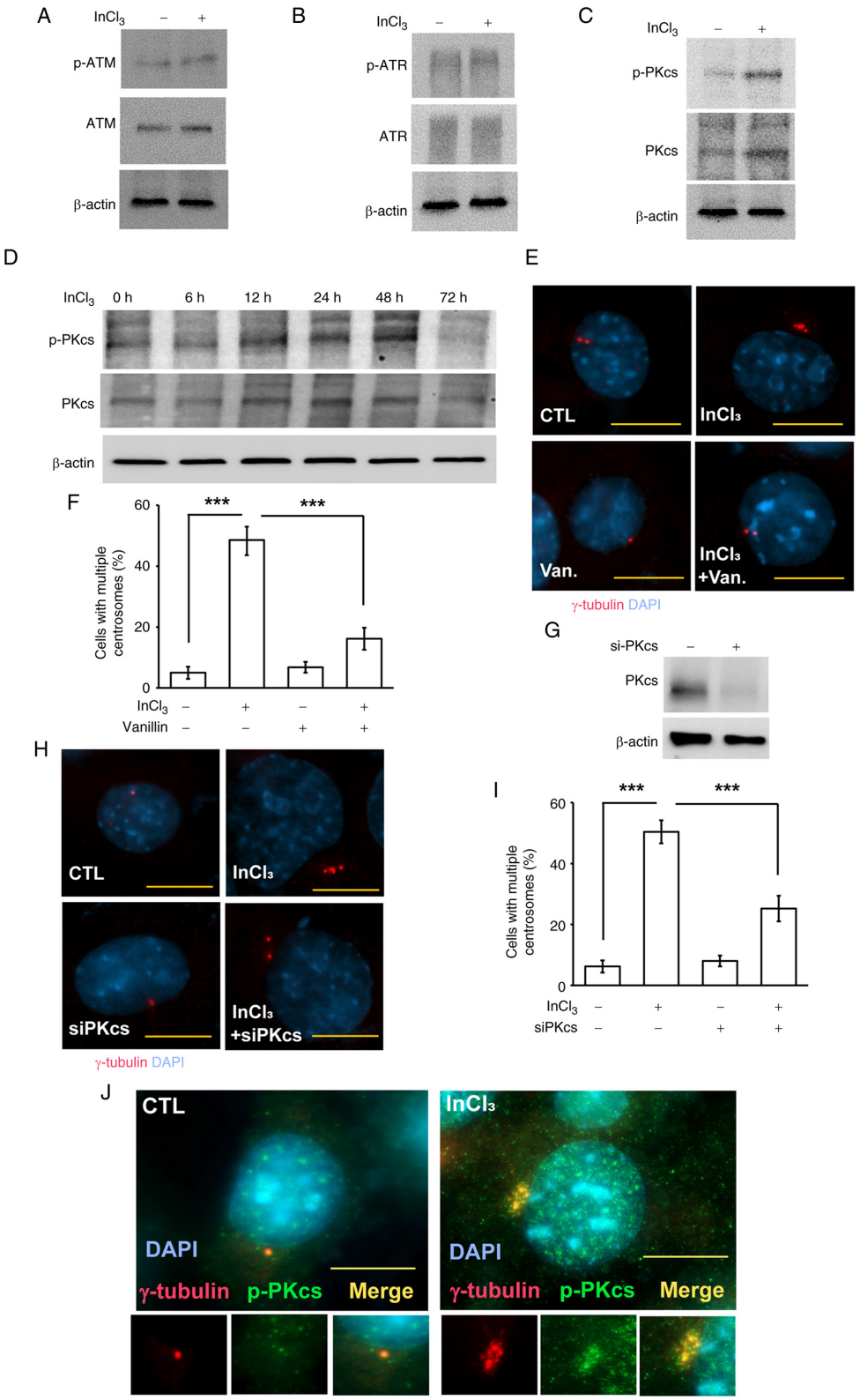

Figure 5. $InCl_3$ activates DNA-PK to facilitate centrosome amplification. DNA-PK, but not ATM and ATR, was activated by $InCl_3$ treatment. Extracts of $InCl_3$-treated TM3 cells were analyzed using western blotting with antibodies against (A) ATM, p-ATM, (B) ATR, p-ATR, (C) DNA-PKcs, p-DNA-PKcs and actin. (D) $InCl_3$ activated DNA-PK in a time-dependent manner. Inhibition or depletion of DNA-PK alleviated centrosome amplification. (E) Representative immunofluorescence images and (F) quantitative results of the proportions of cells with multiple centrosomes in the absence or presence of DNA-PK inhibitor vanillin. Cells were stained with an antibody against γ-tubulin. DNA was counterstained with DAPI. Scale bar, 10 μm. (H) Representative immunofluorescence images and (I) quantitative results of the proportions of cells with multiple centrosomes in the absence or presence of siPKcs. Cells were stained with an antibody against γ-tubulin. DNA was counterstained with DAPI. Scale bar, 10 μm. (G) DNA-PKcs was depleted efficiently. Extracts of cells transfected with siPKcs were examined through western blotting with antibodies against DNA-PKcs and actin. (J) p-DNA-PKcs localized to the centrosome upon $InCl_3$ treatment. Immunofluorescence staining of CTL or $InCl_3$-treated cells with antibodies against γ-tubulin and p-DNA-PKcs. DNA was stained with DAPI. Scale bar, 10 μm. Results are presented as mean ± SD from ≥3 independent experiments. ***P<0.001. DNA-PKcs, DNA-dependent protein kinase catalytic subunit; $InCl_3$, indium chloride; ATM, ataxia telangiectasia mutated; ATR, ATM and Rad3-related Kinase; p-, phosphorylated; CTL, control; siPKcs, small interfering RNA against DNA-PKcs.

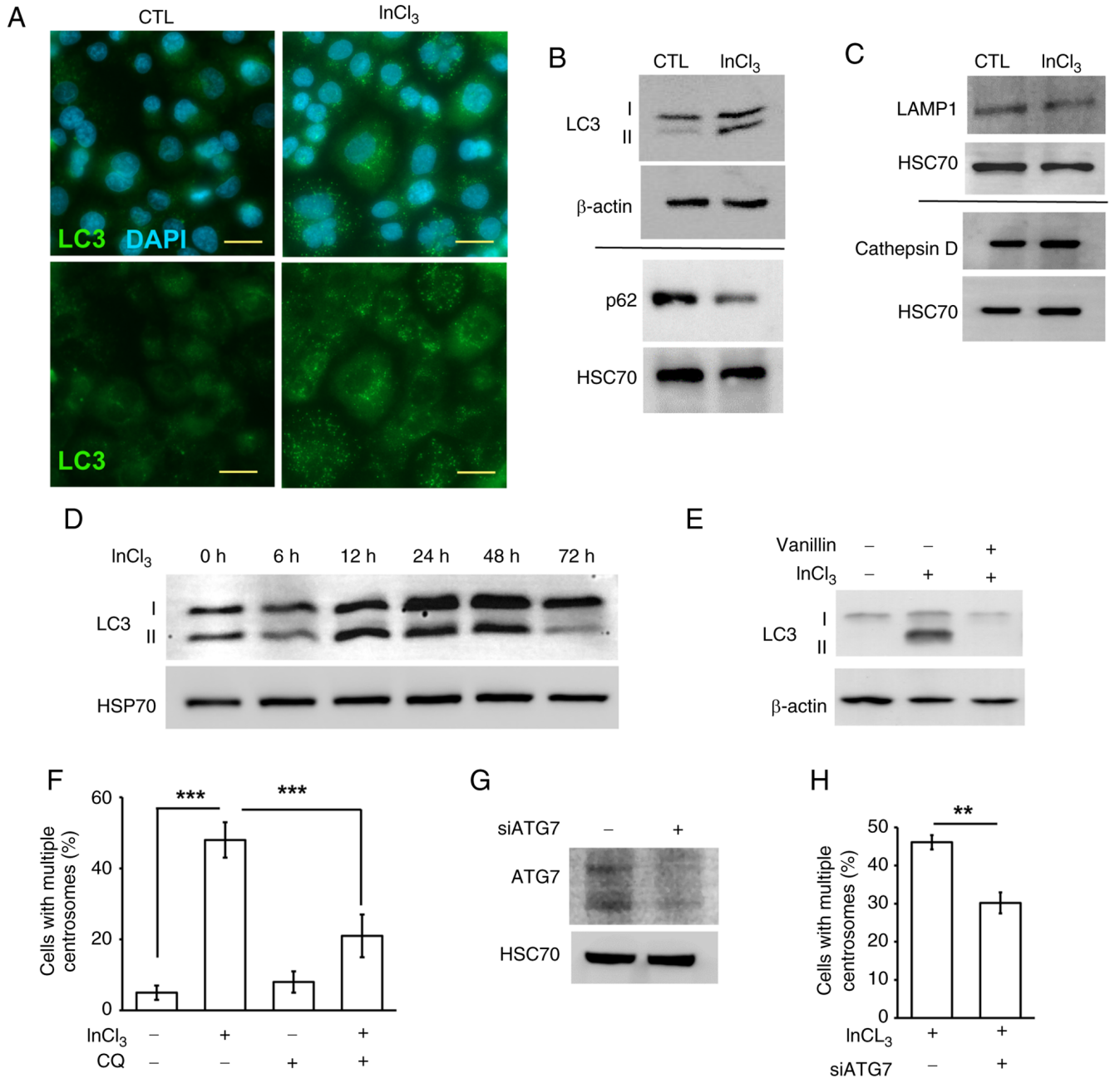

Figure 6. $InCl_3$ induces autophagy to induce centrosome amplification. (A) Immunofluorescence staining of CTL and $InCl_3$-treated cells with antibodies against LC3. DNA was stained with DAPI. Scale bars, 20 μm. (B) Extracts of $InCl_3$-treated cells were analyzed using western blotting with antibodies against LC3, p62, actin and HSC70. (C) Treatment with $InCl_3$ did not alter the expression of lysosomal proteins. Extracts of $InCl_3$-treated cells were analyzed using western blotting with antibodies against LAMP1, cathepsin D and HSC70. (D) $InCl_3$ induced LC3 lipidation in a time-dependent manner. Extracts of InCl3-treated cells at different time periods were analyzed using western blotting with antibodies against LC3 and actin. (E) Inhibition of DNA-PK alleviated InCl3-induced autophagy. Extracts of InCl3-treated cells were analyzed through western blotting with antibodies against LC3 and actin. Inhibition of autophagy or depletion of ATG7 reduced centrosome amplification. (F) Quantitative results of TM3 cells treated with $InCl_3$ in the absence or presence of chloroquine. (G) ATG7 was depleted in TM3 cells transfected with siATG7. Extracts of siATG7-transfected cells were analyzed using western blotting with antibodies against ATG7 and HSC70. (H) Quantitative results of TM3 cells treated with InCl3 in the absence or presence of siATG7. Results are presented as the mean ± SD from ≥3 independent experiments. **P<0.01 and ***P<0.001. $InCl_3$, indium chloride; HSC70, heat shock cognate protein 70; ATG7, autophagy related 7; siATG7, small-interfering RNA against ATG7; DNA-PK, DNA-dependent protein kinase; CTL, control; LAMP1, lysosome-associated membrane protein 1.

Discussion

Consistent with previous reports that indium compounds impair testicular function and sperm quality (10,11), the present study demonstrated that $InCl_3$ inhibits the proliferation of testicular Leydig cells. $InCl_3$ markedly reduced Leydig cell proliferation and caused marked genomic instability. Mechanistically, $InCl_3$ increased intracellular ROS levels, leading to extensive DNA damage, as evidenced by elevated γ-H2AX levels. ROS-mediated DNA damage either promotes DNA-PK activation or autophagy induction to centrosome amplification. These amplified centrosomes became multiple mitotic spindle poles, thereby causing aberrant mitosis and genomic instability. In alignment with prior studies linking

oxidative stress and abnormal centrosome duplication in human HCT116 colon cancer and rat IEC-6 normal small intestine cell lines (42,43), the present findings provide new insights detailing the mechanisms by which $InCl_3$ disrupts Leydig cell proliferation and potentially contributes to male reproductive toxicity.

Human epidemiological data directly associating occupational indium exposure with male reproductive toxicity remain very limited. The majority of available information comes from animal experiments and indirect occupational health observations. Current biomonitoring studies in indium-exposed workers have focused mainly on lung, kidney and liver toxicity and have not systematically evaluated reproductive outcomes (44). By contrast, rodent studies have consistently showed that indium compounds may cause marked testicular injury, including reduced testis weight, vacuolar degeneration, germ-cell loss and abnormal sperm morphology (7). The severity of these effects is associated with serum indium concentrations (10). For example, repeated intratracheal administration of indium compounds in hamsters has resulted in marked reductions in testis and epididymis weights and severe long-lasting testicular lesions (45). To the best of our knowledge, at present, no comparable human data exist regarding testis size or structural damage among indium-exposed workers. Therefore, concerns regarding male reproductive toxicity have been based primarily on animal findings. Although population studies of male infertility in industrial settings suggest that occupational and environmental exposures may contribute to semen abnormalities (9,11,45), a causal association with indium exposure has not been established. Overall, notable animal evidence and general occupational infertility data highlight a potential reproductive risk associated with indium exposure and underscore the need for dedicated human studies in exposed populations.

Although the IC_{50} value of 100 μM used in the present study exceeds the typical levels of environmental or occupational indium exposure, such concentrations are commonly employed in *in vitro* models to elicit detectable cellular responses, due to the absence of systemic metabolism, distribution and clearance mechanisms. A previous study has reported that indium levels in the blood of exposed workers can reach a high ng/ml value (~10^{-8} M) (46), while a further study has demonstrated that indium can accumulate in the lungs and enter systemic circulation, raising concerns about long-term low-dose exposure (47). Furthermore, *in vivo* studies have indicated that indium compounds can induce testicular toxicity. For example, testicular damage and reduced testosterone levels in indium-exposed mice (48). In addition, similar toxic effects were observed in rats following inhalation exposure (49). These findings collectively support the biological plausibility of the present *in vitro* results and highlight the potential reproductive risks associated with indium exposure. Therefore, while the concentration used in the present assays may not directly reflect physiological levels, it serves as a useful model for elucidating the underlying cellular mechanisms involved in indium-induced testicular toxicity. Furthermore, it should be noted that the concentration used in the present study (100 μM) is higher than physiologically relevant levels and thus represents a limitation of the present study. However, such non-physiological doses are often necessary *in vitro* to reveal potential cellular mechanisms that may not be detectable under lower exposure conditions.

Aberrant copy numbers of centrosomes drive mitotic errors and chromosomal instability. Under normal conditions, centrosome duplication is tightly regulated to ensure the formation of a bipolar spindle that accurately segregates chromosomes during mitosis. However, when centrosome amplification occurs, as observed in $InCl_3$-treated Leydig cells, multipolar mitotic spindles are observed, thus leading to chromosome mis-segregation, aneuploidy and genomic instability. Genomic instability imposes a number of consequences on cell physiology. For example, aneuploid or polyploid cells often experience cell cycle arrest, senescence or apoptosis due to activation of the p53-dependent surveillance mechanisms. This aligns with the present observation regarding impaired Leydig cell proliferation following $InCl_3$ exposure. In addition, cells that escape checkpoint control may propagate with abnormal karyotypes, leading to further genetic imbalances and functional decline. Within the context of Leydig cells, which are terminally differentiated endocrine cells responsible for testosterone biosynthesis, persistent genomic instability may compromise the expression of StAR or CYP11A1 enzymes, thereby reducing androgen production. Chronic exposure to $InCl_3$, by continuously inducing centrosome amplification and mitotic defects, gradually depletes the Leydig cell population or renders them functionally incompetent. This, in turn, would disrupt the paracrine signaling network between Leydig and Sertoli cells, leading to defective germ cell maturation and reduced sperm quality.

Genomic instability in somatic testicular cells, including Leydig cells, has been associated with long-term reproductive pathologies. In rodent models, centrosome amplification in the testis is associated with testicular atrophy, decreased sperm count and increased sperm DNA fragmentation, all of which contribute to subfertility or infertility. Given that Leydig cells are relatively quiescent under physiological conditions, the induction of centrosome overduplication and consequent mitotic stress represents a novel mechanism by which $InCl_3$ exerts cumulative damage over time, even at sublethal doses. Taken together, the present study underscores that centrosome amplification is not only a transient cellular aberration but a key event that associates oxidative stress and DNA damage with endocrine dysfunction and reproductive failure. In the broader context of occupational and environmental health, prolonged indium exposure may pose a marked threat to male fertility by targeting Leydig cells, disrupting hormone production and indirectly impairing spermatogenesis. Future studies should aim to investigate whether antioxidant therapies or inhibitors of centrosome overduplication could mitigate these deleterious effects and preserve testicular function in individuals exposed to indium compounds.

The present study demonstrated that DNA-PK, but not ATM or ATR, was selectively activated following $InCl_3$ exposure. This was a key observation as ATM and ATR are considered the canonical kinases in the DNA damage response, with ATM primarily responding to double-strand breaks and ATR responding to replication stress. By contrast, DNA-PK serves a role in non-homologous end joining, directly binding

to DNA ends through the Ku70/Ku80 heterodimer and facilitating DNA repair. The present findings indicate that DNA-PK was the primary activated DDR kinase in Leydig cells upon $InCl_3$ treatment. Notably, DNA-PK phosphorylation was observed not only in the nucleus but also at the centrosome, indicating a non-canonical role in regulating centrosome dynamics. This dual localization highlights the emerging concept that DNA-PK exhibits cytoplasmic functions beyond genome maintenance, particularly in modulating centrosome homeostasis. Furthermore, phosphorylated DNA-PKcs has been previously detected at centrosomes under genotoxic stress (50), where it interacts with key centrosomal proteins such as γ-tubulin, pericentrin and nuclear mitotic apparatus, thereby promoting overduplication and multipolar spindle formation.

The present study observed that pharmacological inhibition or siRNA-mediated depletion of DNA-PKcs significantly alleviated $InCl_3$-induced centrosome amplification, suggesting that aberrant activation of DNA-PKcs in the centrosome promotes centrosome amplification. DNA-PK activation at the centrosome drives centrosome amplification through a number of pathways. One possibility is that DNA-PK phosphorylates centrosome cycle regulators, such as polo-like kinase 4 (PLK4), Aurora A or NIMA-related kinase 2, which are involved in centriole biogenesis and separation (51-53). Alternatively, DNA-PK may contribute to cytoskeletal remodeling by modifying microtubule dynamics (54), indirectly altering centrosome positioning and spindle assembly. Within the context of environmental toxicology, the present study highlights that DNA-PK activation is a key molecular mediator of indium-induced reproductive toxicity, making it a potential therapeutic target.

Although DNA-PKcs has been implicated in regulating centrosome amplification, whether it directly phosphorylates centrosomal proteins such as PLK4 or centrosomal protein 192 kDa (CEP192) remains unclear. Due to the unavailability of phospho-specific antibodies against PLK4 and CEP192 and the low efficiency of immunoprecipitation using anti-PLK4 and anti-CEP192 antibodies, the present study was unable to determine their phosphorylation status. Future studies employing improved detection methods or phospho-proteomic approaches are required to clarify whether DNA-PKcs directly phosphorylates these proteins.

The present study demonstrated that autophagy contributes to $InCl_3$-induced centrosome amplification. Autophagy activation was observed following $InCl_3$ treatment, as evidenced by increased LC3 puncta and conversion of LC3-I to LC3-II. Blocking autophagy with chloroquine significantly reduced centrosome amplification, suggesting that autophagy provides a permissive environment for aberrant centrosome duplication. This finding aligns with previous studies demonstrating that autophagy can promote centrosome amplification in trophoblast and cancer cells (28,34,41). Therefore, ROS-induced autophagy may act synergistically with DNA-PK activation to disrupt centrosome homeostasis.

Collectively, the present findings establish a mechanistic cascade whereby $InCl_3$ generates ROS, which induces DNA damage and activates DNA-PK. Activated DNA-PK accumulates at centrosomes and triggers their amplification. Concurrently, ROS also stimulates autophagy, which further facilitates centrosome amplification. This dual pathway ultimately disrupts mitotic integrity and suppresses Leydig cell proliferation. These findings not only contribute to the current understanding of indium-associated reproductive toxicity but also present novel mechanistic associations between oxidative stress, DNA damage response, autophagy and centrosome homeostasis.

Acknowledgements

The authors would like to thank Professor Wen-Tai Chiu (Bioimaging Core Facility of the National Core Facility for Biopharmaceuticals, Ministry of Science and Technology, Tainan, Taiwan) for their technical support.

Funding

The present study was supported by grants from The National Science and Technology Council of Taiwan (grant no. NSTC-113-2314-B-024-001), The National Cheng Kung University Hospital (grant no. NCKUH-11402027) and The An Nan Hospital, China Medical University (grant no. ANHRF113-36).

Availability of data and materials

The data generated in the present study may be requested from the corresponding author.

Authors' contributions

YNT, CYW, PJS and KCW conceptualized the present study. YNT, CYW, MYK and RCL devised the methodology. PJS and KCW conducted the investigation. RCL and MYK were responsible for software and formal analysis. YNT, CYW and RCL wrote, reviewed and edited the original manuscript. YNT, CYW, PJS and KCW provided supervision and acquired funding for the present study. YNT and CYW confirm the authenticity of all the raw data. All authors read and approved the final version of the manuscript.

Ethics approval and consent to participate

Not applicable.

Patient consent for publication

Not applicable.

Competing interests

The authors declare that they have no competing interests.

References

1. Scansetti G: Exposure to metals that have recently come into use. Sci Total Environ 120: 85-91, 1992.
2. Choi KM and An HC: Characterization and exposure measurement for indium oxide nanofibers generated as byproducts in the LED manufacturing environment. J Occup Environ Hyg 13: D23-D30, 2016.

3. Cummings KJ, Virji MA, Park JY, Stanton ML, Edwards NT, Trapnell BC, Carey B, Stefaniak AB and Kreiss K: Respirable indium exposures, plasma indium, and respiratory health among indium-tin oxide (ITO) workers. Am J Ind Med 59: 522-531, 2016.
4. Sato A, Saito K, Abe K, Sugimoto K, Nagao T, Sukeda A and Yunaiyama D: Indium chloride bone marrow scintigraphy for hepatic myelolipoma: A case report. World J Clin Cases 11: 4377-4383, 2023.
5. Eskandari A, Glerum DM and Tsui TY: Influence of Indium (III) chloride on human dermal fibroblast cell adhesion on tantalum/silicon oxide Nano-composites. Materials (Basel) 15: 3577, 2022.
6. Kimura E, Ahmed S, Chen H and Hiraku Y: Epithelial-mesenchymal transition in human alveolar cells exposed to indium chloride. J Appl Toxicol 45: 2353-2362, 2025.
7. Tsai PK, Wu SW, Chiang CY, Lee MW, Chen HY, Chen WY, Chen CJ, Yang SF, Yeh CB and Kuan YH: Evaluation of cytotoxicity, apoptosis, and genotoxicity induced by indium chloride in macrophages through mitochondrial dysfunction and reactive oxygen species generation. Ecotoxicol Environ Saf 193: 110348, 2020.
8. Manno RA, Grassetti A, Oberto G, Nyska A and Ramot Y: The minipig as a new model for the evaluation of doxorubicin-induced chronic toxicity. J Appl Toxicol 36: 1060-1072, 2016.
9. Bomhard EM: The toxicology of indium oxide. Environ Toxicol Pharmacol 58: 250-258, 2018.
10. Lee KH, Chen HP, Leung CM, Chen HL, Tsai SS and Hsu PC: Effects of indium chloride exposure on sperm morphology and DNA integrity in rats. J Food Drug Anal 23: 152-160, 2015.
11. Lee KH, Chen HL, Leung CM, Chen HP and Hsu PC: Indium acetate toxicity in male reproductive system in rats. Environ Toxicol 31: 68-76, 2016.
12. Teves ME and Roldan ERS: Sperm bauplan and function and underlying processes of sperm formation and selection. Physiol Rev 102: 7-60, 2022.
13. Chen HB, Pineda Garcia JC, Arizono S, Takeda T, Li RS, Hattori Y, Sano H, Miyauchi Y, Hirota Y, Tanaka Y and Ishii Y: DAPL1 is a novel regulator of testosterone production in Leydig cells of mouse testis. Sci Rep 11: 18532, 2021.
14. Walker WH: Testosterone signaling and the regulation of spermatogenesis. Spermatogenesis 1: 116-120, 2011.
15. Collin F: Chemical basis of reactive oxygen species reactivity and involvement in neurodegenerative diseases. Int J Mol Sci 20: 2407, 2019.
16. Gottschling BC, Maronpot RR, Hailey JR, Peddada S, Moomaw CR, Klaunig JE and Nyska A: The role of oxidative stress in indium phosphide-induced lung carcinogenesis in rats. Toxicol Sci 64: 28-40, 2001.
17. Brun NR, Christen V, Furrer G and Fent K: Indium and indium tin oxide induce endoplasmic reticulum stress and oxidative stress in zebrafish (Danio rerio). Environ Sci Technol 48: 11679-11687, 2014.
18. Cheng SM, Shieh MC, Lin TY and Cheung CHA: The 'Dark Side' of autophagy on the maintenance of genome stability: Does it really exist during excessive activation? J Cell Physiol 237: 178-188, 2022.
19. Blackford AN and Jackson SP: ATM, ATR, and DNA-PK: The Trinity at the Heart of the DNA damage response. Mol Cell 66: 801-817, 2017.
20. Shiloh Y and Ziv Y: The ATM protein kinase: Regulating the cellular response to genotoxic stress, and more. Nat Rev Mol Cell Biol 14: 197-210, 2013.
21. Fokas E, Prevo R, Hammond EM, Brunner TB, McKenna WG and Muschel RJ: Targeting ATR in DNA damage response and cancer therapeutics. Cancer Treat Rev 40: 109-117, 2014.
22. Wang CY, Huang EY, Huang SC and Chung BC: DNA-PK/Chk2 induces centrosome amplification during prolonged replication stress. Oncogene 34: 1263-1269, 2015.
23. Filomeni G, De Zio D and Cecconi F: Oxidative stress and autophagy: The clash between damage and metabolic needs. Cell Death Differ 22: 377-388, 2015.
24. Codogno P and Meijer AJ: Autophagy and signaling: Their role in cell survival and cell death. Cell Death Differ 12 (Suppl 2): S1509-S1518, 2005.
25. Kim J, Kundu M, Viollet B and Guan KL: AMPK and mTOR regulate autophagy through direct phosphorylation of Ulk1. Nat Cell Biol 13: 132-141, 2011.
26. Ichimura Y, Kirisako T, Takao T, Satomi Y, Shimonishi Y, Ishihara N, Mizushima N, Tanida I, Kominami E, Ohsumi M, *et al*: A ubiquitin-like system mediates protein lipidation. Nature 408: 488-492, 2000.
27. Wang CY, Kao YH, Lai PY, Chen WY and Chung BC: Steroidogenic factor 1 (NR5A1) maintains centrosome homeostasis in steroidogenic cells by restricting centrosomal DNA-dependent protein kinase activation. Mol Cell Biol 33: 476-484, 2013.
28. Teng YN, Chang HC, Chao YY, Cheng HL, Lien WC and Wang CY: Etoposide triggers cellular senescence by inducing multiple centrosomes and primary cilia in adrenocortical tumor cells. Cells 10: 1466, 2021.
29. Lai PY, Wang CY, Chen WY, Kao YH, Tsai HM, Tachibana T, Chang WC and Chung BC: Steroidogenic Factor 1 (NR5A1) resides in centrosomes and maintains genomic stability by controlling centrosome homeostasis. Cell Death Differ 18: 1836-1844, 2011.
30. Livak KJ and Schmittgen TD: Analysis of relative gene expression data using real-time quantitative PCR and the 2(-Delta Delta C(T)) method. Methods 25: 402-408, 2001.
31. Tsai YC, Kuo TN, Chao YY, Lee PR, Lin RC, Xiao XY, Huang BM and Wang CY: PDGF-AA activates AKT and ERK signaling for testicular interstitial Leydig cell growth via primary cilia. J Cell Biochem 124: 89-102, 2023.
32. Wang CY, Hong YH, Syu JS, Tsai YC, Liu XY, Chen TY, Su YM, Kuo PL, Lin YM and Teng YN: LRWD1 regulates microtubule nucleation and proper cell cycle progression in the human testicular embryonic carcinoma cells. J Cell Biochem 119: 314-326, 2018.
33. Lin RH, Yang ML, Li YC, Chang HM and Kuan YH: Indium chloride-induced micronuclei via reactive oxygen species in Chinese hamster lung fibroblast V79 cells. Environ Toxicol 28: 595-600, 2013.
34. Lin RC, Chao YY, Lien WC, Chang HC, Tsai SW and Wang CY: Polo-like kinase 1 selective inhibitor BI2536 (dihydropteridinone) disrupts centrosome homeostasis via ATM-ERK cascade in adrenocortical carcinoma. Oncol Rep 50: 167, 2023.
35. Tsai YC, Kuo TN, Chao YY, Lin RC, Chien HH, Peng IT, Tsai YF, Su PJ and Wang CY: Pericentriolar material 1 aggregation maintains cell survival upon prolonged replication stress. Arch Biochem Biophys 768: 110383, 2025.
36. Wang CY, Tsai SW, Chien HH, Chen TY, Sheu SY, So EC and Huang BM: Cordycepin inhibits human gestational choriocarcinoma cell growth by disrupting centrosome homeostasis. Drug Des Devel Ther 14: 2987-3000, 2020.
37. Chao YY, Huang BM, Peng IC, Lee PR, Lai YS, Chiu WT, Lin YS, Lin SC, Chang JH, Chen PS, *et al*: ATM- and ATR-induced primary ciliogenesis promotes cisplatin resistance in pancreatic ductal adenocarcinoma. J Cell Physiol 237: 4487-4503, 2022.
38. Chen TY, Huang BM, Tang TK, Chao YY, Xiao XY, Lee PR, Yang LY and Wang CY: Genotoxic stress-activated DNA-PK-p53 cascade and autophagy cooperatively induce ciliogenesis to maintain the DNA damage response. Cell Death Differ 28: 1865-1879, 2021.
39. Wang CY, Lai PY, Chen TY and Chung BC: NR5A1 prevents centriole splitting by inhibiting centrosomal DNA-PK activation and beta-catenin accumulation. Cell Commun Signal 12: 55, 2014.
40. Lien WC, Chen TY, Sheu SY, Lin TC, Kang FC, Yu CH, Kuan TS, Huang BM and Wang CY: 7-hydroxy-staurosporine, UCN-01, induces DNA damage response, and autophagy in human osteosarcoma U2-OS cells. J Cell Biochem 119: 4729-4741, 2018.
41. Tsai YC, Kuo TN, Lin RC, Tsai HL, Chao YY, Lee PR, Su PJ and Wang CY: MicroRNA-155-5p inhibits trophoblast cell proliferation and invasion by disrupting centrosomal function. Mol Med Rep 29: 85, 2024.
42. Bian XK, Guo JL, Xu SX, Han YW, Lee SC and Zhao JZ: Hexavalent chromium induces centrosome amplification through ROS-ATF6-PLK4 pathway in colon cancer cells. Cell Biol Int 46: 1128-1136, 2022.
43. Zhang RK, Wang P, Lu YC, Lang L, Wang L and Lee SC: Cadmium induces cell centrosome amplification via reactive oxygen species as well as endoplasmic reticulum stress pathway. J Cell Physiol 234: 18230-18248, 2019.
44. Hoet P, De Graef E, Swennen B, Seminck T, Yakoub Y, Deumer G, Haufroid V and Lison D: Occupational exposure to indium: What does biomonitoring tell us? Toxicol Lett 213: 122-128, 2012.
45. Tanaka A: Health effects of indium compounds in animal experiments. J Occup Health 67: uiaf007, 2025.
46. Choi S, Won YL, Kim D, Yi GY, Park JS and Kim EA: Subclinical interstitial lung damage in workers exposed to indium compounds. Ann Occup Environ Med 25: 24, 2013.
47. Ding CG, Wang HQ, Song HB, Li ZH, Li XP, Ye SS, Zhang FG, Cui SW, Yan HF and Li T: Occupational exposure to indium of indium smelter workers. Biomed Environ Sci 29: 379-384, 2016.

48. Nagano K, Nishizawa T, Umeda Y, Kasai T, Noguchi T, Gotoh K, Ikawa N, Eitaki Y, Kawasumi Y, Yamauchi T, *et al*: Inhalation carcinogenicity and chronic toxicity of indium-tin oxide in rats and mice. J Occup Health 53: 175-187, 2011.
49. Maghraoui S, Florea A, Ayadi A, Matei H and Tekaya L: Changes in organ weight, sperm quality and testosterone levels after aluminum (Al) and indium (In) administration to Wistar rats. Biol Trace Elem Res 201: 766-775, 2023.
50. Zhang S, Hemmerich P and Grosse F: Centrosomal localization of DNA damage checkpoint proteins. J Cell Biochem 101: 451-465, 2007.
51. Zhou K, He Y, Lin X, Zhou H, Xu X and Xu J: KIFC1 depends on TRIM37-mediated ubiquitination of PLK4 to promote centrosome amplification in endometrial cancer. Cell Death Discov 10: 419, 2024.
52. Qi H, Kikuchi M, Yoshino Y, Fang Z, Ohashi K, Gotoh T, Ideta R, Ui A, Endo S, Otsuka K, *et al*: BRCA1 transports the DNA damage signal for CDDP-induced centrosome amplification through the centrosomal Aurora A. Cancer Sci 113: 4230-4243, 2022.
53. Bobbitt JR, Cuellar-Vite L, Weber-Bonk KL, Yancey MR, Majmudar PR and Keri RA: Targeting the mitotic kinase NEK2 enhances CDK4/6 inhibitor efficacy by potentiating genome instability. J Biol Chem 301: 108196, 2025.
54. Ma S, Rong Z, Liu C, Qin X, Zhang X and Chen Q: DNA damage promotes microtubule dynamics through a DNA-PK-AKT axis for enhanced repair. J Cell Biol 220: e201911025, 2021.